Charles E. Spritzer, MD • Norbert J. Pelc, ScD[2] • James N. Lee, PhD • Avery J. Evans, MD • H. Dirk Sostman, MD • Stephen J. Riederer, PhD

Rapid MR Imaging of Blood Flow with a Phase-Sensitive, Limited-Flip-Angle, Gradient Recalled Pulse Sequence: Preliminary Experience[1]

To assess blood flow rapidly, a limited-flip-angle, gradient recalled pulse sequence was modified to acquire two views at the same phase-encoding step in successive repetitions. One view is obtained with first-moment flow compensation, while the second view is obtained with selectable flow encoding (nonzero first moment) along one direction. Blood flowing along the encoded direction acquires a phase difference between the two views, resulting in signal dependent on both direction and speed of flow. Stationary tissues undergo no phase change. Therefore, the phase shift between the two views produces an image that spatially renders flow direction and velocity. With a 24-msec repetition time, a 256 × 128 matrix, and two excitations, data acquisition is completed in 13 seconds per location (both a magnitude image and a flow image are produced at each location). Images generated with flow phantoms confirmed the accuracy of this method. Preliminary clinical evidence in 23 human subjects suggests that this method is useful in evaluating portal hypertension, distinguishing arterial from venous flow, distinguishing between slow flow and clot, and confirming the presence of clot. This method appears to be a fast, easy way to assess blood flow in large vessels.

Index terms: Aorta, flow dynamics, 948.92 • Aorta, MR studies, 89.1214, 948.1299 • Knee, MR studies, 459.1214 • Magnetic resonance (MR), pulse sequences • Magnetic resonance (MR), rapid imaging • Magnetic resonance (MR), technology • Portal vein, MR studies, 957.1214 • Portal vein, thrombosis, 957.751 • Thrombosis, MR studies • Venae cavae, MR studies, 982.1214 • Venae cavae, 982.751

Radiology 1990; 176:255–262

BECAUSE of its sensitivity to flowing blood, magnetic resonance (MR) imaging has been used to evaluate the cardiovascular system, to confirm vessel patency and course, to identify and characterize intraluminal masses or a clot, and to document vascular dissections and aneurysms (1–10).

It is well known that the appearance of flowing blood is a complex function of both rheologic dynamics and the chosen pulse sequence (11–15). Although an understanding of flow phenomena may facilitate the separation of intraluminal signal due to flowing blood from that of intravascular tumor or thrombus, uncertainty often remains. Misinterpretation of tumor or clot as a flow "artifact" or vice versa may alter clinical diagnosis and management (16,17). With spatial presaturation and flow compensation techniques, an attempt is made to minimize the variability of flow phenomena on spin-echo (SE) images by producing respectively more consistent flow void or intraluminal signal (18–20). These techniques, although certainly an improvement, do not completely eliminate all potentially confusing flow phenomena.

Limited-flip-angle (LFA), gradient recalled echo techniques such as fast low angle shot (FLASH) and gradient recalled acquisition in a steady state (GRASS) are increasingly being used to assess vascular pathologic conditions because of their speed and ease of implementation and the intrinsically high contrast available between flowing blood and stationary tissues (9,21,22). On LFA images, coherently flowing blood has high signal intensity because fully magnetized protons continuously enter the section and replace partially saturated spins and because there is no spatially selective 180° pulse to discriminate against flowing spins. Phase images derived from SE data sets have been shown to be reliable in separating flow phenomena from intraluminal masses (17,23–25). Although some phase mapping techniques make it possible to measure the speed and direction of flowing fluids by means of MR imaging, many of these techniques are time consuming because of the need to obtain *n* independent images in order to encode *n* independent values of flow (26–29). O'Donnell suggested a more efficient SE technique to measure blood velocity, whereby only two views per phase-encoding step are acquired (30). One view is a conventional SE acquisition, the other view includes a bipolar flow-encoding gradient. The phase difference between the two views measures the flow velocity along the axis of the flow-encoding gradient. We have modified this technique and adapted it to LFA acquisitions. Images reflecting the presence, direction, and velocity of blood flow can be obtained in 13 seconds, with spatial resolution comparable with that on standard MR images.

[1] From the Department of Radiology, Duke University Medical Center, PO Box 3808, Durham, NC 27710 (C.E.S., A.J.E., H.D.S.); GE Medical Systems, Milwaukee (N.J.P.); the Department of Radiology, University of Utah, Salt Lake City (J.N.L.); and the Department of Radiology, Mayo Clinic, Rochester, Minn (S.J.R.).
From the 1988 RSNA annual meeting. Received May 4, 1989; revision requested June 8; revision received March 6, 1990; accepted March 19. Supported in part by National Institutes of Health grant HL37310 and by GE Medical Systems, Milwaukee. **Address reprint requests to** C.E.S.

[2] Current address: Department of Radiology, Stanford University, Stanford, CA.

Abbreviations: EDTA = ethylenediaminetetraacetic acid, FLASH = fast low angle shot, GRASS = gradient recalled acquisition in a steady state, LFA = limited flip angle, SE = spin echo, TE = echo time, TR = repetition time, VIGRE = velocity imaging with gradient recalled echoes.

THEORY

The data acquired with conventional imaging pulse sequences produce an array wherein the value at each voxel is a complex quantity. This complex value can be represented in Cartesian coordinates (real and imaginary parts) or in polar coordinates (magnitude and phase). The magnitude of the complex value in each voxel is the amount of net transverse magnetization contained in that voxel when an echo is produced in a view with no phase encoding. The phase of the complex number is the relative angle at which the magnetization is pointed at that time. In most pulse sequences, the magnitude is used to form the image, and the phase is discarded.

The phase of a complex image may contain contributions from several sources. Details of the pulse sequence timing can cause slowly varying phase shifts throughout the image, as can magnetic fields generated by eddy currents. Radio-frequency penetration effects also produce spatially dependent phase shifts, while magnetic field inhomogeneities affect phase in LFA images. Finally, motion in the presence of magnetic field gradients can also induce phase shifts.

It is well known that moving nuclei develop a phase shift in the presence of balanced gradients (eg, a bipolar gradient with a net area of zero), while stationary spins do not (12,30,31). This phase shift is proportional to the product of the flow velocity and the first moment of the gradient waveform (20,32,33). In a two-dimensional Fourier transform image, such phase shifts can produce multiple discrete "ghosts" displaced along the phase-encoding axis. The application of appropriately chosen additional gradients along the section-selection and/or readout direction can prevent these ghosts. This produces high intraluminal signal and makes the image acquisition insensitive to velocity (or acceleration and pulsatility if more complicated gradient waveforms are applied). These gradient modifications are known commonly as flow compensation gradients, motion artifact suppression technique, or simply moment-nulled gradient waveforms (19,20,32).

O'Donnell proposed an SE technique to measure the velocity of flowing fluids in which two views per phase-encoding gradient increment were acquired (30). The first view used a bipolar flow-encoding gradient, whereas the second view

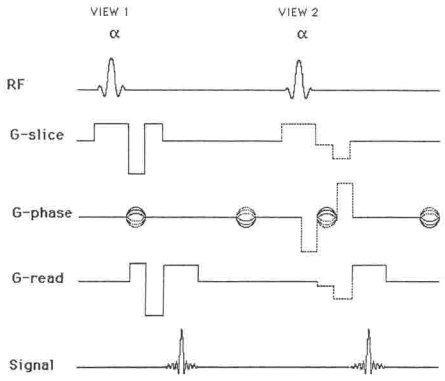

Figure 1. Pulse sequence in velocity imaging with gradient recalled echoes (VIGRE). *View 1* incorporates first-order flow compensation. As drawn, *View 2* has flow encoding on all three axes. In practice, only flow encoding along one axis is enabled. Note that the equivalent of a bipolar pulse is incorporated into the conventional imaging lobes whenever possible so as to minimize echo time (TE). α = flip angle, *G-phase* = phase-encoding gradient, *G-read* = read-out gradient, *G-slice* = section-encoding gradient, *RF* = radio frequency.

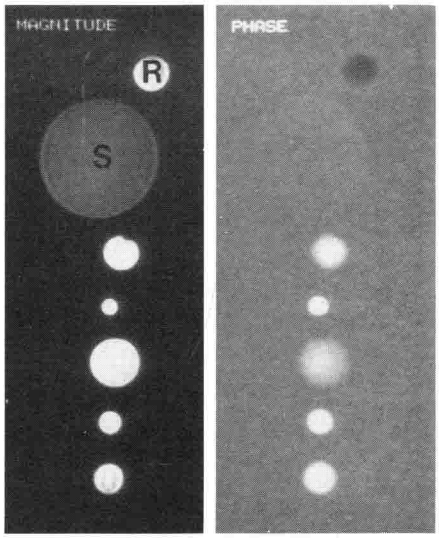

a. **b.**

Figure 2. Flow phantom. **(a)** Magnitude image generated from *View 1* data. The five lower tubes are connected in series with the fluid flowing into the picture. A standard (*S*) separates these tubes from the return tube (*R*), which has fluid flowing in the opposite direction. A conventional GRASS image would look identical. **(b)** VIGRE flow image. Fluid flowing into the picture (the five interconnected tubes) appears white, while fluid flowing in the reverse direction appears black. Stationary fluid (the standard) has no signal. Note that faster flowing fluid (small tubes) appears brighter than slower fluid.

was obtained without this gradient pulse. The second set of views produces a conventional image in which the (complex) signal intensity in a voxel is a function of spin density, T1, T2, and the aforementioned phase effects. The first set of data depends on all the above and also includes an additional phase shift secondary to velocity. The phase difference ($\Delta\phi$) between the two resulting images is

$$\Delta\phi = \gamma \Delta m v$$

where Δm is the change in the gradient's first moment (with respect to time) due to the modified bipolar pulse, v is the velocity, and γ is the gyromagnetic ratio. The moment is calculated by integrating the gradient pulse shape and timing with respect to time. Thus, the phase difference between the two images for any given pixel is related directly to flow velocity along the axis of the applied bipolar pulse.

This method may be applied to a limited-flip-angle, gradient recalled pulse sequence. We modified a standard GRASS technique, acquiring two views per phase encoding increment. A pulse sequence diagram is shown in Figure 1. One view uses the standard first-moment flow compensation gradient, and the second view has a selectable (nonzero) first-moment flow compensation gradient. Data for two complete images are acquired. The first has velocity flow compensation, making it exactly equivalent to a conventional GRASS sequence. It is insensitive to the motion-induced phase differences produced by flowing blood. The phase in each pixel of the second image differs from that in the first image by an amount dependent on flow speed and direction. Thus, the flow-compensated acquisition is used as a phase reference for the flow-encoded acquisition. The direction and sensitivity of the flow encoding is selected by the operator. If it is assumed that all spins in a given voxel have the same velocity (a reasonable assumption for cross-sectional imaging), then the phase shift between the two images is proportional to velocity in the encoded direction. Conversely, a large variation in velocities within a voxel will produce an average phase shift indicative of the average velocity within the image voxel (34); Martin AJ, personal communication, 1989.

The precision with which the velocity can be measured depends on the signal magnitude. With LFA methods, regions containing flow have high signal intensity, and visibility of the vasculature may be enhanced by multiplying the phase-difference image by the magnitude of the flow-compensated image. In the

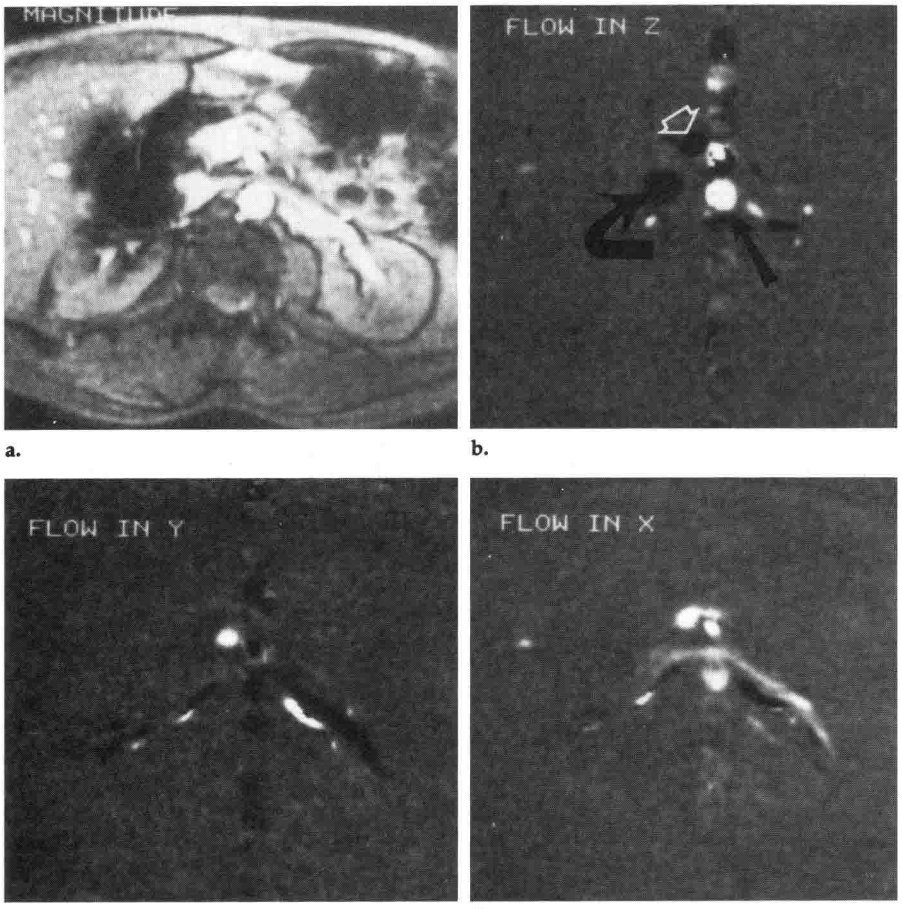

Figure 3. Images of blood flow in a healthy volunteer. **(a)** Transaxial magnitude image demonstrates the renal veins. **(b)** VIGRE image shows encoded flow in the cranial-caudal direction. Flow in the aorta (straight solid arrow) is displayed in white, while opposing flow in the inferior vena cava (curved arrow) and portal vein (open arrow) is shown in black. **(c)** VIGRE flow image obtained from the anteroposterior direction. The renal veins and the renal arteries are black. **(d)** Flow image encoding from side to side. Blood moving toward the right (eg, left renal vein) is encoded in white.

resulting image, static structures are suppressed because they exhibit no phase shift and usually have lower signal intensity than flowing blood. Thus, in the present implementation, two images are produced at each section location. One is a flow-compensated magnitude image exactly equivalent to that obtained with a conventional GRASS sequence. The second image is proportional to the product of magnitude and velocity (Figs 2, 3). Quantitative flow information can be retrieved from the two images.

This technique is called velocity imaging with gradient recalled echoes (VIGRE). With a repetition time (TR) of 24 msec, a TE of 13 msec, a 256 × 128 matrix, and two excitations, the two images may be acquired in less than 13 seconds, providing information about fluid speed and direction along the velocity-encoding axis. In principle, when two additional flow-encoding views are acquired at each phase-encoding step, velocity information could be obtained in all three orthogonal planes in as little as 26 seconds.

SUBJECTS AND METHODS

All images were obtained on a 1.5-T clinical imager (Signa; GE Medical Systems, Milwaukee).

Phantom Studies

The accuracy of flow velocity determined with VIGRE was studied with two phantoms.

Steady state flow.—For steady state flow, the device consisted of five serially connected tubes of varying inner diameters, thereby producing a range of flow velocities (Fig 2). The fluid contained gadolinium chloride-ethylenediaminetetraacetic acid (EDTA), which produced a T1 relaxation time similar to that of blood (approximately 600 msec). Steady state flow rates varied over a range of 2–65 mL/sec. Corresponding velocities ranged from 1 to 30 cm/sec.

Pulsatile flow.—A pulsatile phantom was constructed to enable more accurate evaluation of in vivo flow patterns. The device consisted of three serially connected tubes with varying inner diameters. The fluid, like the fluid used to assess steady state flow, contained $GdCl_3$-EDTA. Average flow rates were 0–27 mL/sec. The corresponding average velocities ranged from 0 to 38 cm/sec. The phantom "heart rate" varied from 51 to 73 beats per minute. Reproducibility was assessed by obtaining four, five, or six acquisitions at two section locations for each flow rate. At each acquisition, average flow was measured with a graduated cylinder.

Clinical Studies

Patient population.—One healthy volunteer and 23 patients were evaluated with VIGRE images. Twelve female and 12 male subjects 2 months to 74 years old were studied. Anatomic regions included the lower-extremity venous system (seven subjects); the aorta, inferior vena cava, and renal veins (seven subjects); the portal system (three subjects); the sagittal sinus (two subjects); the carotid artery (one subject); the superior vena cava and subclavian veins (two subjects); one patient with an arteriovenous malformation in the spinal cord; and one patient with an aneurysm of the ulnar artery.

Clinical indications.—VIGRE imaging was used to validate the technique in four subjects (one volunteer and three patients with known vessel patency or thrombus); in 20 subjects, VIGRE was used in a prospective manner to evaluate clinical questions. In nine subjects, VIGRE was used to distinguish slow flow from an intraluminal clot or mass. The portal system was assessed in three subjects to determine patency and flow direction. In three subjects, clot with high signal intensity was suspected. In three subjects, confirmation of a patent vascular structure as arterial or venous was necessary for correct interpretation of the standard images; in another three subjects, VIGRE imaging was used in an attempt to identify feeding or draining vessels.

In this feasibility study, VIGRE data were acquired when interpretation of conventional magnitude images was unable to resolve the question at hand. For example, VIGRE images were acquired when the possibility of slow flow could not be distinguished from intraluminal clot. Accordingly, a direct comparison of VIGRE data and data acquired with conventional pulse sequences would be inappropriate because the patient population was highly selected. It is more informative to consider how often VIGRE images added useful clinical data. If the VIGRE data established the diagnosis or correctly changed the interpretation of the study from an equivocation to a definite opinion, VIGRE data were believed to confirm the diagnosis. If the VIGRE data agreed with the interpretation based on conventional pulse sequences but did not estab-

lish the diagnosis or increase the confidence level of the diagnosis, the VIGRE images were believed to support the original MR imaging diagnosis. Failure to accomplish these objectives resulted in VIGRE data being considered not useful, and a misdiagnosis ascribed to VIGRE information was noted as such.

Reference studies.—In the clinical patients, confirmation by venography or arteriography was available in 16 patients, computed tomography (CT) in three patients, Doppler or color flow ultrasound (US) in two patients, and a radionuclide flow study in one patient, for a combined total of 22 patients. In the remaining patient, endoscopy suggested the presence of esophageal and gastric varices. SE images with long TRs (TR msec/TE msec = 2,000 or 2,500/20, 40, or 80) and short-TR images (500 or 600/15, 20, or 25) were available in 14 and 19 patients, respectively; conventional sequentially acquired GRASS images (33/13, flip angle = 45°–70°) were obtained in each instance.

Technique.—A 24-msec TR, 13-msec TE, 30° flip angle, 10-mm-thick section, 256 × 128 matrix, and two excitations were used in each instance. The field of view varied from 48 to 24 cm, depending on the area being imaged. With these parameters, imaging time was 13 seconds per section. The direction or directions of flow to be encoded were chosen to best address the clinical concern. Our choice of the first moment of the flow-encoded views was based on knowledge of gradient strength and duration, so that the anticipated maximum velocity to be imaged produced a 180° phase shift. Slower velocities produce proportionately smaller phase deviations. Maximum velocities for the clinical studies were chosen on a trial-and-error basis, depending on experience with our volunteer and the first three patients. If the presence of slow flow was to be confirmed, maximum velocities of 20–60 cm/sec were selected. If flow direction was to be determined, maximum velocities of 60–100 cm/sec were chosen.

RESULTS

Phantom Studies

Steady state flow.—For the range of constant velocities used in this experiment, the calculated velocities from the VIGRE images enabled accurate measurement of the true velocities. The correlation coefficient was $r = 0.99$; the VIGRE calculated velocity was 0.116 cm/sec ± 1.01 × (actual velocity) (Fig 4).

Pulsatile flow.—The VIGRE images enabled accurate measurement of average velocities from 0 to 38 cm/sec. The correlation coefficient was $r = 0.99$; the calculated average velocity was 1.3 cm/sec ± 1.05 × (actual average velocity) (Fig 5).

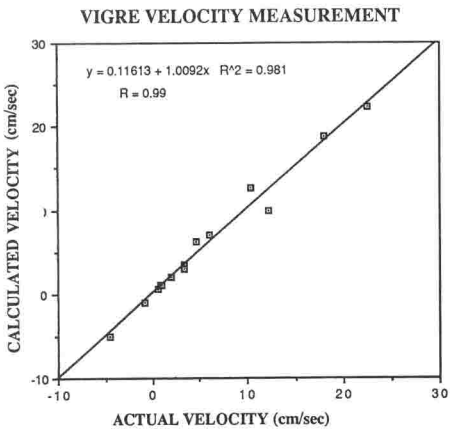

4.

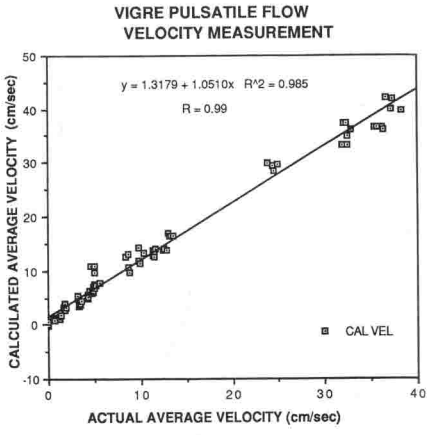

5.

Figures 4, 5. **(4)** Graph compares flow velocities measured with a VIGRE pulse sequence with actual velocities in a linear flow phantom. **(5)** Average flow velocities measured with VIGRE pulse sequence are compared with the actual average velocities in a pulsatile flow phantom. *CAL VEL* = calculated average velocity.

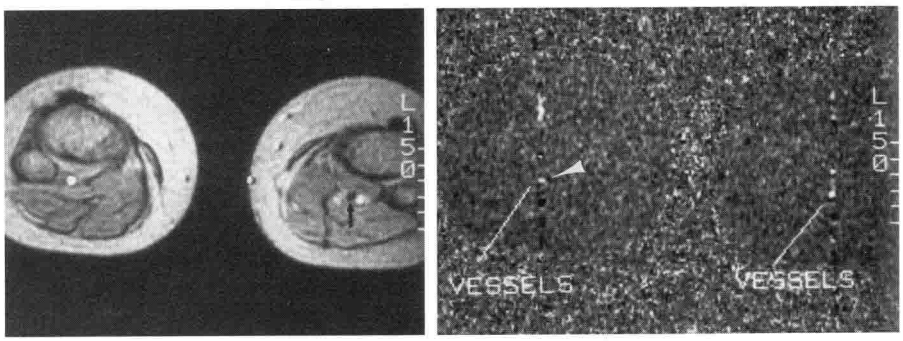

a. b.

Figure 6. Images of a 31-year-old woman with left-sided deep venous thrombosis. **(a)** GRASS image in the popliteal region confirms clot (arrow) in left popliteal vein. However, the right popliteal vein is not visualized; thus, a clot may be present in it. **(b)** Flow image depicts the right popliteal vein as a small black dot (arrowhead) adjacent to the white artery.

Clinical Studies

The results are summarized in the Table. The VIGRE flow images were useful in enabling distinction between slow flow and clot in six of nine subjects in whom it was used for this purpose. In two of the remaining nine subjects, the VIGRE images agreed with the interpretation of the standard pulse sequences but did not increase the certainty of the diagnosis. In the ninth subject, pulsation artifact obscured the vessel of interest.

The VIGRE data confirmed the presence of a thrombus with high signal intensity that would have been difficult to diagnose on GRASS and/or SE images in two of three studies. Although they enabled us to separate thrombi with high signal intensity from blood flow, VIGRE images did not improve confidence levels in the third study.

In two subjects, VIGRE display of flow direction confirmed that a vessel was arterial or venous. Hepatopetal or hepatofugal flow and portal/splenic vein patency was confirmed in three subjects.

The VIGRE images failed to enable detection of one spinal arteriovenous malformation and small draining veins associated with a soft-tissue tumor. Standard pulse sequences also failed to enable detection of these abnormalities.

DISCUSSION

Many investigators have implemented fluid flow measurements with magnetic resonance since the idea was first proposed by Hahn in 1960 (17,23,24,26–28,30,31). Unfortunately, standard SE implementation to flow imaging has suffered from lengthy data acquisition or low signal-to-noise ratios (26,27,30).

We adapted and modified the O'Donnell technique for use with limited-flip-angle, gradient recalled echoes (30).

A similar technique for producing

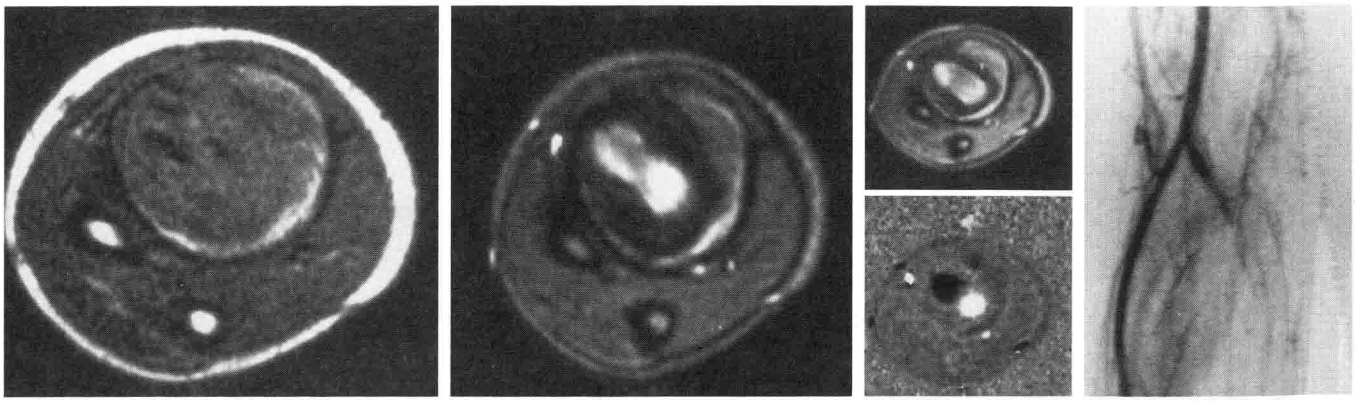

a. b. c. d.

Figure 7. Images of 26-year-old woman with a false aneurysm, arising from the ulnar artery. **(a)** SE image (500/20) shows soft-tissue mass. **(b)** GRASS image (33/13, with a 45° flip angle) with high signal intensity at the periphery of the aneurysm as well as centrally. Clot with high signal intensity cannot be separated from flowing blood. **(c)** VIGRE magnitude (top) and flow (bottom) images confirm that the central high signal intensity is due to swirling blood; the peripheral high signal intensity is due to thrombus. **(d)** Digital subtraction angiogram confirms the presence of an aneurysm.

Results of Clinical Studies in 24 Subjects

Purpose of VIGRE	Total (Studies Available)	VIGRE Results Confirm Diagnosis*	VIGRE Results Support Diagnosis†
Confirm technique (would determine flow direction and identify occluded vessels)	4‡	NA	NA
Separate slow flow from clot/mass	9	6	2
Diagnose thrombus with high signal intensity	3	2	1
Identify structure as artery or vein	2	2	0
Assess portal patency and flow direction	3	3	0
Identify feeding or draining vessels	3	0	0

Note.—NA = not applicable.

* VIGRE acquisition established the diagnosis or correctly changed interpretation of the study from equivocal to more definite.

† VIGRE agreed with the interpretation based on the conventional pulse sequences but did not enable diagnosis or increase confidence level of the diagnosis.

‡ Includes one healthy volunteer without confirmatory study.

MR angiograms has recently been described (35). Flow-compensated and flow-uncompensated magnitude images are reconstructed and subtracted to produce an angiogram. This technique does not encode flow direction and velocity (as does VIGRE) because phase information is not preserved. An alternative angiographic technique that is able to quantitate blood flow has been described by Dumoulin and Hart (36) and Dumoulin et al (37) for detection and quantification obtained with bipolar flow-encoding gradients.

Flow phenomena produce an intraluminal signal that may be confused with a mass or thrombus on SE images (1,9,17,25). LFA pulse sequences that produce magnitude images may be performed quickly and generally provide excellent contrast between flowing blood and intraluminal clot or soft tissue. However, slowly flowing blood itself may become partially saturated, resulting in decreased signal intensity mimicking an intraluminal mass (9). Conversely, the high signal intensity of some thrombi may be difficult to differentiate from the high signal intensity of flowing blood (38). VIGRE is a technique that potentially combines the specificity of SE phase images with the speed of LFA imaging.

When conventional LFA techniques are used, slowly flowing blood becomes partially saturated, resulting in less signal. This area of decreased signal intensity may be misinterpreted as intraluminal mass or clot (9). In six of nine examinations performed to distinguish slow flow from clot, VIGRE images confirmed the presence or absence of thrombus where GRASS and/or SE images were equivocal (Fig 6). Although the VIGRE images supported the interpretations of the standard sequences in an additional two studies, the diagnosis or the confidence level of the interpretations was not significantly altered by the phase-difference images. In the remaining subject, pulsation artifact obscured visualization of the vessel of interest on the flow images.

In a soft-tissue tumor, VIGRE images did not enable detection of very slowly draining veins shown by angiography. The images were acquired with a 30° flip angle and a 10-mm section thickness. Preliminary phantom studies and clinical experience have shown that the sensitivity to very slow flow may be improved by decreasing section thickness, increasing flip angle, and enlarging flow encoding gradients; nonetheless, the threshold for detecting slow flow is unclear. In this subject, SE and GRASS images likewise failed to enable identification of the draining veins.

The signal characteristics of intraluminal thrombus depend on composition, the spin state of hemoglobin, the presence or absence of red blood cell lysis, and the field strength of the imager. Because both the composition and form of heme products vary over time, thrombus may have either high or low signal intensity on SE and LFA images (9,34,39,40). In this series, three patients had an intraluminal thrombus with high signal intensity that was depicted on GRASS images and confirmed with other imaging modalities. In two of the three patients, VIGRE established the presence of clot (Fig 7). In the third patient, VIGRE images enabled the correct interpretation, but both T1- and T2-weighted SE images were considered sufficient to enable the correct diagnosis. VIGRE appears to be a reliable means of separating clot with high signal intensity from flowing blood.

Data acquired with a flow phantom

show that VIGRE enables accurate measurement of average velocity and direction in steady state flow. With the use of the magnitude image to measure the cross-sectional area of a vessel, volume flow rates (area multiplied by average velocity) may be determined readily when the flow is in the section direction. With pulsatile flow, average flow rates may be established, although the correlation is not as precise as in the steady state case. When this technique is modified to resemble cine MR imaging, it should provide accurate data about both average and instantaneous blood flow (41).

Determination of the direction of flow in a vessel is usually a useful means of distinguishing between an artery and a vein. In one case of possible deep venous thrombosis, VIGRE images confirmed that a solitary vessel was arterial, established that the occluded vessel was a vein, and thus substantiated the diagnosis of deep venous thrombosis. In a second patient with possible deep venous thrombosis, assessment of flow direction confirmed that the solitary vessel seen was the popliteal vein, not (as originally suspected) the popliteal artery. The presence of deep venous thrombosis was excluded, and unnecessary anticoagulation was obviated.

In this pilot study, the phase images established hepatopetal or hepatofugal flow and confirmed vessel patency shown on conventional LFA images in the three patients evaluated for portal vein thrombosis, portal hypertension, or both (Figs 8, 9). If these preliminary results are validated in a larger prospective study, MR imaging could become an even more valuable tool in the assessment of hepatic dysfunction because it would be able to simultaneously provide (*a*) information about hepatic tumors currently obtained with CT and (*b*) vascular information now acquired with US or angiography.

In a patient with a spinal arteriovenous malformation, the vessels were not visualized on the VIGRE images because of technical difficulties, poor resolution due to the large field of view, and flowing cerebrospinal fluid that obscured the arteriovenous malformation.

In this preliminary study, VIGRE images did not contradict findings of any magnitude imaging, but we believe that the phase information confirmed the interpretation of MR images in 13 subjects, possibly obviating a confirmatory study.

The limitations of VIGRE include its sensitivity to gradient imperfections. Eddy currents induced by the gradients used to encode flow can cause different phase shifts in the two images and therefore a residual phase error (Fig 9). Our recent experience indicates these may be overcome by the use of shielded gradients, phase correction algorithms, or both.

An additional problem concerns the choice of the nonzero first moment. Whereas signal phase can only be uniquely defined in the range ± 180°, flow velocities greater than the assumed maximum velocity cause phase shifts outside this range. For example, if a maximum encoded velocity of 50 cm/sec is selected, spins moving at 60 cm/sec acquire more than 180° of phase shift and appear to have a velocity of −40 cm/sec (Fig 10). Using a smaller first moment increases the maximum velocity not subject to aliasing but has the disadvantage of reducing sensitivity to slow flow. Accordingly, if flow direction is the pertinent concern, we use smaller gradient values; to confirm slow flow, we use larger gradient values. It may be possible to combine information from multiple experiments to increase the dynamic range of flow velocity without sacrificing sensitivity (30). Also, it may be possible to invoke phase continuity to unwrap phase aliasing (42).

Pulsatile flow may also be a problem with the present method. Although the imaging data collected with the flow-compensated views are relatively consistent and produce artifact-free images, the flow-encoded data may produce artifacts. The prob-

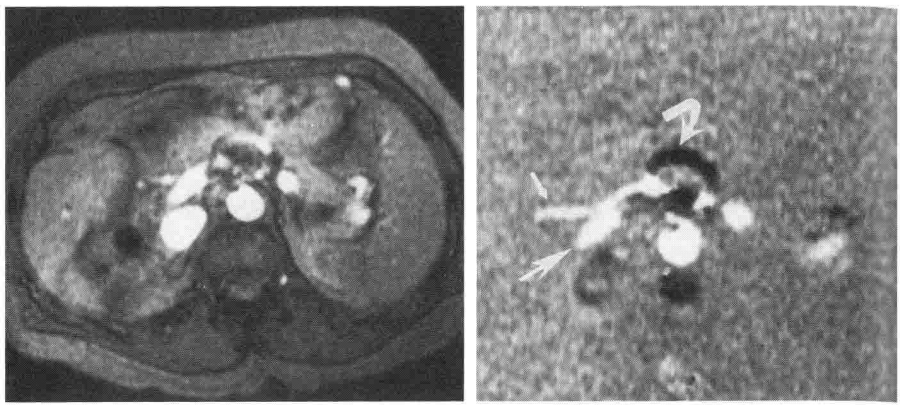

a. b.

Figure 8. Images of 67-year-old woman, obtained after construction of distal splenorenal shunt. **(a)** Magnitude GRASS image shows patency of the portal vein. **(b)** The flow image confirms patency and demonstrates flow toward the liver (shown in white) in both the hepatic artery (small straight arrow) and portal vein (large straight arrow). Flow in the opposite direction, as seen in the splenic artery (curved arrow), is black.

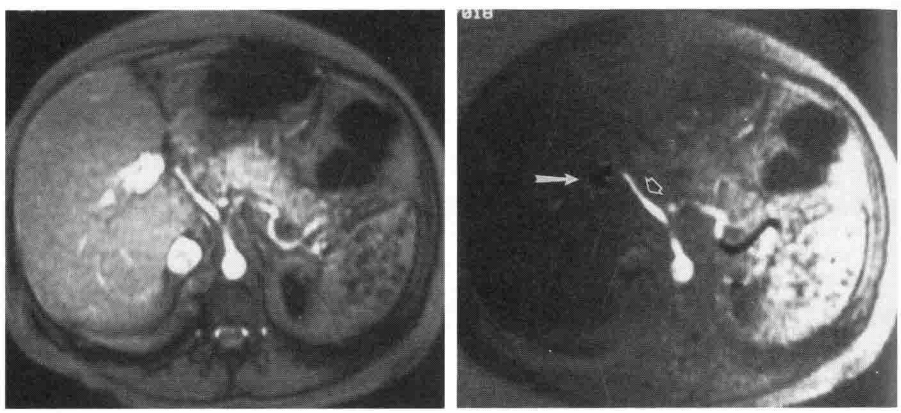

a. b.

Figure 9. Unconfirmed study of 50-year-old woman with paroxysmal nocturnal hemoglobinuria and possible portal vein thrombosis and hypertension demonstrates the influence of eddy currents on the VIGRE flow image. **(a)** Magnitude image shows no significant shading. Portal vein patency is evident. **(b)** VIGRE flow image. Marked shading is indicative of phase instability, presumably caused by eddy currents. Note that this image suggests hepatofugal (black) flow (solid arrow). The hepatopetal flow of the hepatic artery is white (open arrow).

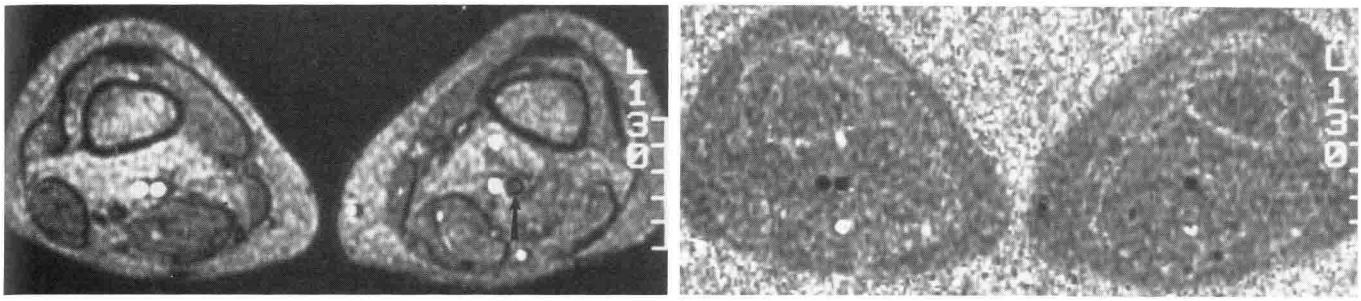

a. b.

Figure 10. Images of 67-year-old woman with left-sided deep venous thrombosis. **(a)** Magnitude image confirms clot on left (arrow). **(b)** Flow image obtained with flow encoding adjusted to detect slow flow. No flow is evident in the thrombosed left popliteal vein. However, on the asymptomatic right side, blood in the vein and blood in the artery appear to be flowing in the same direction. The rapid flow in the popliteal artery results in a greater than 180° phase shift, causing aliasing of the flow direction.

lem stems directly from the flow encoding itself. Pulsatile fow causes the signal from a voxel to have an inconsistent phase throughout the collected data. These unexpected phase shifts cause the signal from the voxel to be dispersed in the phase-encoded direction. The flow information within the pulsatile vessel is therefore suspect, although the vessel can be assumed to be arterial. The artifacts extending from the vessel can obscure vessels of interest. Changing the phase and frequency-encoding directions can minimize the effect of extraluminal ghosts. However, a gated technique will be necessary to evaluate the more pulsatile central vessels. Such a technique is currently under development (41).

As with any flow mapping acquisition, turbulence remains a problem. The random dephasing caused by such complex flow results in loss of velocity and directional information. Additionally, because VIGRE is an LFA method that does not use a 180° refocusing pulse, it suffers from the same sensitivity to magnetic susceptibility as conventional LFA pulse sequences.

A final limitation concerns the resolution achievable with VIGRE. On our system, all LFA acquisitions were limited to a 24-cm field of view. The corresponding in-plane resolution is 0.9 mm × 1.9 mm for a 256 × 128 matrix. Data generated from vessels approaching these dimensions should be suspect. Although the section thickness used in the current study was 10 mm, we now routinely use a 7-mm section thickness. Sections thinner than 7 mm produce phase errors due to gradient nonlinearity.

In conclusion, this preliminary study suggests that VIGRE holds promise for quickly determining flow direction and velocity as well as distinguishing between slow flow and clots. It also appears useful for confirming the presence of intraluminal thrombus with high signal intensity. Larger prospective studies will be necessary to assess its clinical utility in detail. ■

Acknowledgments: The authors thank Jerry Dahlke for his assistance in constructing our pulsatile flow phantom.

References

1. Crooks L, Mills C, David P, et al. Visualization of cerebral and vascular abnormalities by NMR imaging: the effects of imaging parameters on contrast. Radiology 1982; 144:843–852.
2. Amparo E, Higgins C, Hoddick W, et al. Magnetic resonance imaging of aortic disease: preliminary results. AJR 1984; 143:1203–1209.
3. Braun I, Hoffman J Jr, Malko J, Pettigrew R, Dannels W, David P. Jugular venous thrombosis: MR imaging. Radiology 1985; 157:357–360.
4. Dinsmore R, Liberthson R, Wismer G, et al. Magnetic resonance imaging of thoracic aortic aneurysms: comparison with other imaging methods. AJR 1986; 146:309–314.
5. Dinsmore R, Wedeen V, Miller S, et al. MRI of dissection of the aorta: recognition of the intimal tear and differential flow velocities. AJR 1986; 146:1286–1288.
6. Fein A. Lee J, Balfe D, et al. Diagnosis and staging of renal cell carcinoma: a comparison of MR imaging and CT. AJR 1987; 148:749–753.
7. McMurdo K, de Geer G, Webb W, Gamsu G. Normal and occluded mediastinal veins: MR imaging. Radiology 1986; 159:33–38.
8. Liberman J, Alfidi R, Nelson A, et al. Gated magnetic resonance imaging of the normal and diseased heart. Radiology 1984; 152:465–470.
9. Spritzer CE, Sussman S, Blinder R, Saeed M, Herfkens RJ. Deep venous thrombosis evaluation with limited flip angle, gradient-refocused MR imaging: preliminary experience. Radiology 1988; 166:371–375.
10. Spritzer CE, Herfkens RJ. Cardiovascular disease and MRI. In: Kressel HY, ed. Magnetic resonance annual, 1988. New York: Raven, 1988; 217–244.
11. Axel L. Blood flow effects in magnetic resonance imaging. AJR 1984; 143:1157–1166.
12. Bradley W Jr, Waluch V, Lai K, Fernandez E, Spalter C. The appearance of rapidly flowing blood on magnetic resonance images. AJR 1984; 143:1167–1174.
13. Bradley W Jr, Waluch V. Blood flow: magnetic resonance imaging. Radiology 1985; 154:443–450.
14. von Schulthess G, Higgins C. Blood flow imaging with MR: spin-phase phenomena. Radiology 1985; 157:687–695.
15. Carr H, Purcell E. Effects of diffusion on free precession in nuclear magnetic resonance experiments. Phys Rev 1954; 94:630–638.
16. Mills C, Brant-Zawadzki M, Crooks L, et al. Nuclear magnetic resonance: principles of blood flow imaging. AJR 1984; 142:165–170.
17. von Schulthess G, Augustiny N. Calculation of T2 values versus phase imaging for the distinction between flow and thrombus in MR imaging. Radiology 1987; 164:549–554.
18. Felmlee J, Ehman R. Spatial presaturation: a method for suppressing flow artifacts and improving depiction of vascular anatomy in MR imaging. Radiology 1987; 164:559–564.
19. Edelman R, Atkinson D, Silver M, Loaiza F, Warren W. FRODO pulse sequences: a new means of eliminating motion, flow, and wraparound artifacts. Radiology 1988; 166:231–236.
20. Pattany P, Phillips J, Chiu L, et al. Motion artifact suppression technique (MAST) for MR imaging. J Comput Assist Tomogr 1987; 11:369–377.
21. Frahm J, Merboldt K, Hanicke W, Haase A. Flow suppression in rapid FLASH NMR images. Magn Reson Med 1987; 4:372–377.
22. Wehrli F. Introduction to fast scan magnetic resonance. General Electric Publication 7299. Milwaukee: GE Medical Systems, 1987.
23. Dinsmore R, Wedeen V, Rosen B, Wismer G, Miller S, Brady T. Phase-offset technique to distinguish slow blood flow and thrombus on MR images. AJR 1987; 148:634–636.
24. Wedeen V, Rosen B, Chesler D, Brady T. MR velocity imaging by phase display. J Comput Assist Tomogr 1985; 9:530–536.
25. White E, Edelman R, Wedeen V, Brady T. Intravascular signal in MR imaging: use of phase display for differentiation of blood-flow signal from intraluminal disease. Radiology 1986; 161:245–249.
26. Wedeen V, Rosen B, Buxton R, Brady T. Projective MRI angiography and quantitative flow-volume densitometry. Magn Reson Med 1986; 3:226–241.

27. Wedeen VJ, Rosen BR, Brady TJ. Magnetic resonance angiography. In: Kressel HY, ed. Magnetic resonance annual, 1987. New York: Raven, 1987:113–178.
28. Singer J. Blood flow rates by nuclear magnetic resonance measurements. Science 1959; 130:1652–1653.
29. Moran PR. A flow zeugmatographic interlace for NMR imaging in humans. Magn Reson Imaging 1982; 1:197.
30. O'Donnell M. NMR blood flow imaging using multiecho, phase contrast sequences. Med Phys 1985; 12:59–64.
31. Hahn EL. Detection of sea-water motion by nuclear precession. J Geophys Res 1960; 65:776.
32. Haacke EM, Lenz G. Improving MR image quality in the presence of motion by using rephasing gradients. AJR 1987; 148:1251–1258.
33. Pattany P, Marino R, McNally J. Velocity and acceleration desensitization in 2DFT MR imaging. Magn Reson Imaging 1966; 4:154.
34. Moran PR, Moran RA, Karstaedt N. Verification and evaluation of internal flow and motion. Radiology 1985; 154:433–441.
35. Lee JN, Reiderer SJ, Pelc NJ. Flow compensated limited flip angle angiography. Magn Reson Med (in press).
36. Dumoulin CL, Hart HR Jr. Magnetic resonance angiography. Radiology 1986; 161:717–720.
37. Dumoulin CL, Souza SP, Hart HR. Rapid scan magnetic resonance angiography. Magn Reson Med 1987; 5:238–245.
38. Atlas SW, Grossman RI, Hackney DB, Goldberg HI, Bilaniuk LT, Zimmerman RA. MR imaging of intracranial vascular lesions using fast imaging (abstr). Radiology 1987; 165(P):217.
39. Rapoport S, Sostman H, Pope C, Camputaro C, Holcomb W, Gore J. Venous clots: evaluation with MR imaging. Radiology 1987; 162:527–530.
40. Braun I, Hoffman J Jr, Malko J, Pettigrew R, Dannels W, Davis P. Jugular venous thrombosis: MR imaging. Radiology 1985; 157:357–360.
41. Pelc NJ, Shimakawa A, Glover HG. Phase contrast cine MRI (abstr). Presented at the Eighth Annual Meeting and Exhibition of the Society of Magnetic Resonance in Medicine, Amsterdam, August, 1989.
42. Axel L, Morton D. Correction of phase wrapping in magnetic resonance imaging. Med Phys 1989; 16:284–287.